ACS NANO

www.acsnano.org

ARTICLE

Hierarchical Porous Film with Layer-by-Layer Assembly of 2D Copper Nanosheets for Ultimate Electromagnetic Interference Shielding

Ho Kwang Choi, Aram Lee, Mina Park, Dong Su Lee, Sukang Bae, Seoung-Ki Lee, Sang Hyun Lee, Takhee Lee, and Tae-Wook Kim*

Cite This: *ACS Nano* 2021, 15, 829−839

Read Online

ACCESS | Metrics & More | Article Recommendations | Supporting Information

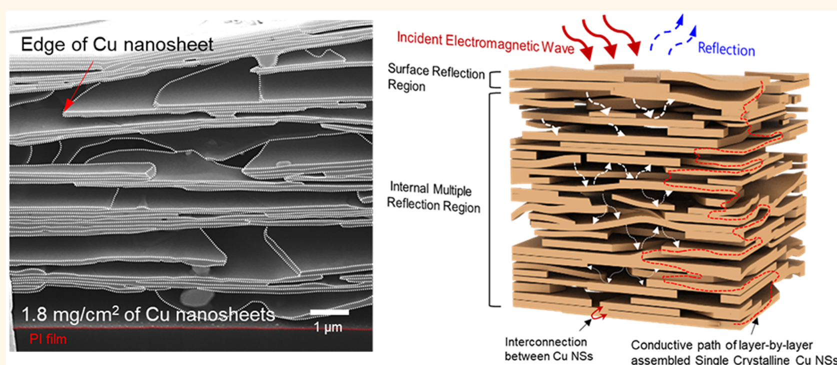

ABSTRACT: The emergence of technologies, such as 5G telecommunication, electric vehicles, and wearable electronics, has prompted demand for ultrahigh-performance and cost-effective shielding materials to protect against both the potentially harmful effects of electromagnetic interference (EMI) on human health and electronic device operation. Here, we report hierarchical porous Cu foils via an assembly of single-crystalline, nanometer-thick, and micrometer-long copper nanosheets and their use in EMI shielding. Layer-by-layer assembly of Cu nanosheets enabled the formation of a hierarchically structured porous Cu film with features such as multilayer stacking; two-dimensional networking; and a layered, sheetlike void architecture. The hierarchical-structured porous Cu foil exhibited outstanding EMI shielding performance compared to the same thickness of dense copper and other materials, exhibiting EMI shielding effectiveness (SE) values of 100 and 60.7 dB at thicknesses of 15 and 1.6 μm, respectively. In addition, the EMI SE of the hierarchical porous Cu film was maintained up to 18 months under ambient conditions at room temperature and showed negligible changes after thermal annealing at 200 °C for 1 h. These findings suggest that Cu nanosheets and their layer-by-layer assembly are one of the promising EMI shielding technologies for practical electronic applications.

KEYWORDS: *copper nanosheet, single-crystalline, 2D metallic nanomaterials, hierarchal structure, porous foil, electromagnetic interference shielding*

Since the invention of the first electronic system at the beginning of the 20th century, electronic equipment has become smaller and faster.[1] With the development of mobile and telecommunication technology, electromagnetic radiation has attracted great interest due to its harmful effects on electronic circuitry and its potential effects on human health.[2−6] Current research and development in wearable smart devices, 5G telecommunication, and electric vehicles

Received: September 1, 2020
Accepted: January 6, 2021
Published: January 11, 2021

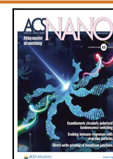

© 2021 American Chemical Society

https://dx.doi.org/10.1021/acsnano.0c07352
ACS Nano 2021, 15, 829−839

Downloaded via SEOUL NATL UNIV on January 3, 2022 at 12:10:56 (UTC).
See https://pubs.acs.org/sharingguidelines for options on how to legitimately share published articles.

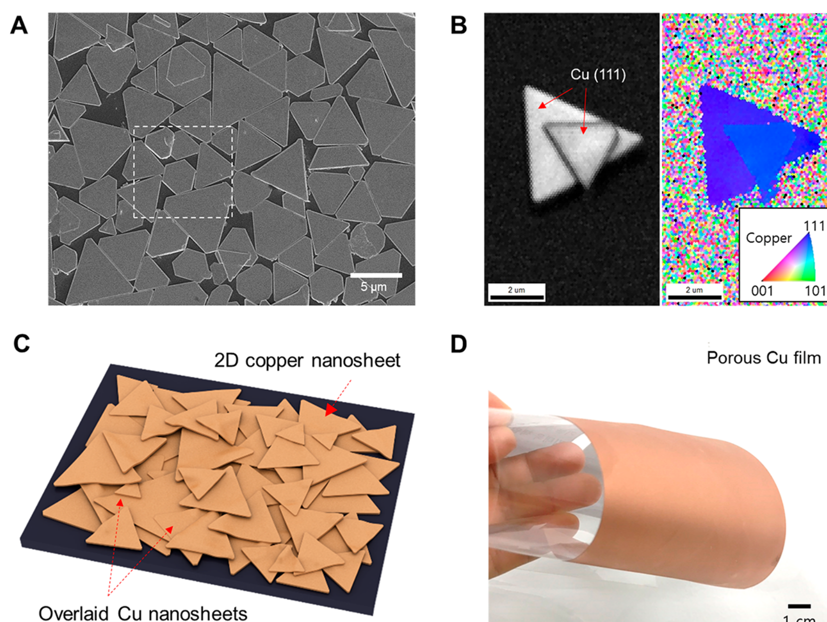

Figure 1. Structural characteristics of Cu NSs and their resulting films. (a) SEM image of monolayer Cu NSs on a SiO_2 substrate. (b) EBSD analysis of single-crystalline Cu NSs showing that the basal plane of the nanosheet is (111). (c) Schematic of large-area single-crystalline Cu NSs piled on each other to form conductive films. (d) Large porous Cu NSs film on a plastic substrate (the total size is 15.5 cm × 15.5 cm).

requires effective shielding or minimization of electromagnetic pollution.[6,7]

The conventional strategy to address electromagnetic interference (EMI) relies on various materials that isolate or separate the targets from the electromagnetic wave source through different mechanisms, such as reflection or absorption.[8−10] The interface between two electrically conductive materials that differ considerably in impedance has been proven effective at reflecting electromagnetic waves. Specific materials with strong electron or magnetic poles that interact with electromagnetic waves can reduce EMI effects by absorption. Multiple internal reflections from a constructed internal scattering architecture or defective points in shielding materials are considered a third shielding mechanism.[9−12]

The most widely used and cost-efficient EMI shielding materials are conductive materials, such as metal-based thin films, foils, and meshes.[1,2,9,10] Conductive filler materials and polymer composites have been intensively studied as core systems for EMI shielding films and packaging due to their advantages (light weight, high performance, and easy processability).[3] Carbon-based conductive nanofillers, including carbon nanotubes, reduced graphene oxide, and graphene, and their thin films have been applied to EMI shielding films as substitutes for metallic materials.[13−22]

Micro- or nanoarchitecturing of internal structures of the shielding films is another approach to enhance EMI shielding effectiveness (SE). This approach generally leads to multiple internal reflections by maximizing the travel path of the electromagnet (EM) in a shielding system. Microsphere structures that are composed of hollow spherical cores and conductive shells have been intensively studied.[23−25] Those porous films with spherical internal architectures have been prepared by complicated extra coatings of metallic materials (Ni, Cu, Co, Ag, or carbon-based two-dimensional (2D) nanomaterials).[26−29] Although those films exhibited enhanced EMI SE performance compared to conventional dense metallic films or foils, advanced architecturing of the internal structure and material design was required to achieve an extraordinary shielding performance with a high reliability.

In this paper, we report a porous Cu foil that is processed by a macro-assembly of single-crystalline copper nanosheets. Because of their structure, the large metal sheets are vertically stacked to simultaneously create a multilayered 2D architecture and sheetlike voids. The hierarchical-structured porous Cu foil exhibited outstanding EMI shielding performance compared to the same thickness of dense copper and other materials, showing EMI SE values of 100 and 60.7 dB at thicknesses of 15 and 1.6 μm, respectively. We identify that the internal hierarchical structure contributes to outstanding EMI shielding performance of the porous Cu foil from scanning electron microscopy (SEM), three-dimensional (3D) X-ray tomography, and a finite-difference time-domain (FDTD) numerical simulation. In addition, the EMI SE of the hierarchical porous Cu film was maintained up to 18 months under ambient conditions at room temperature and showed negligible changes after thermal annealing at 200 °C for 1 h. These experimental results set EMI SE records for the performance of both synthetic materials with the same loading weight per unit area and pure metal foils. Moreover, large 2D copper nanosheets (Cu NSs) have numerous advantages, such as low cost, easy synthesis, easy processing, light weight, thin, and mechanical softness, that are appealing for emerging EMI SE materials.

RESULTS AND DISCUSSION

Copper nanosheets, that is, large-area, sheet-shaped metallic fillers with micron-sized edge length and nanometer-scale thicknesses, were synthesized by a simple hydrothermal method. Their structural characteristics allow Cu nanosheets to be used as a conductive filler for electrodes and enabled an overlaid architecture that can cover a desired two-dimensional substrate. Figure 1a shows SEM and electron backscattering diffraction (EBSD) images of copper nanosheets on a substrate. Because of their two-dimensional shape, copper nanosheets are easily placed on the substrate individually as

https://dx.doi.org/10.1021/acsnano.0c07352
ACS Nano 2021, 15, 829−839

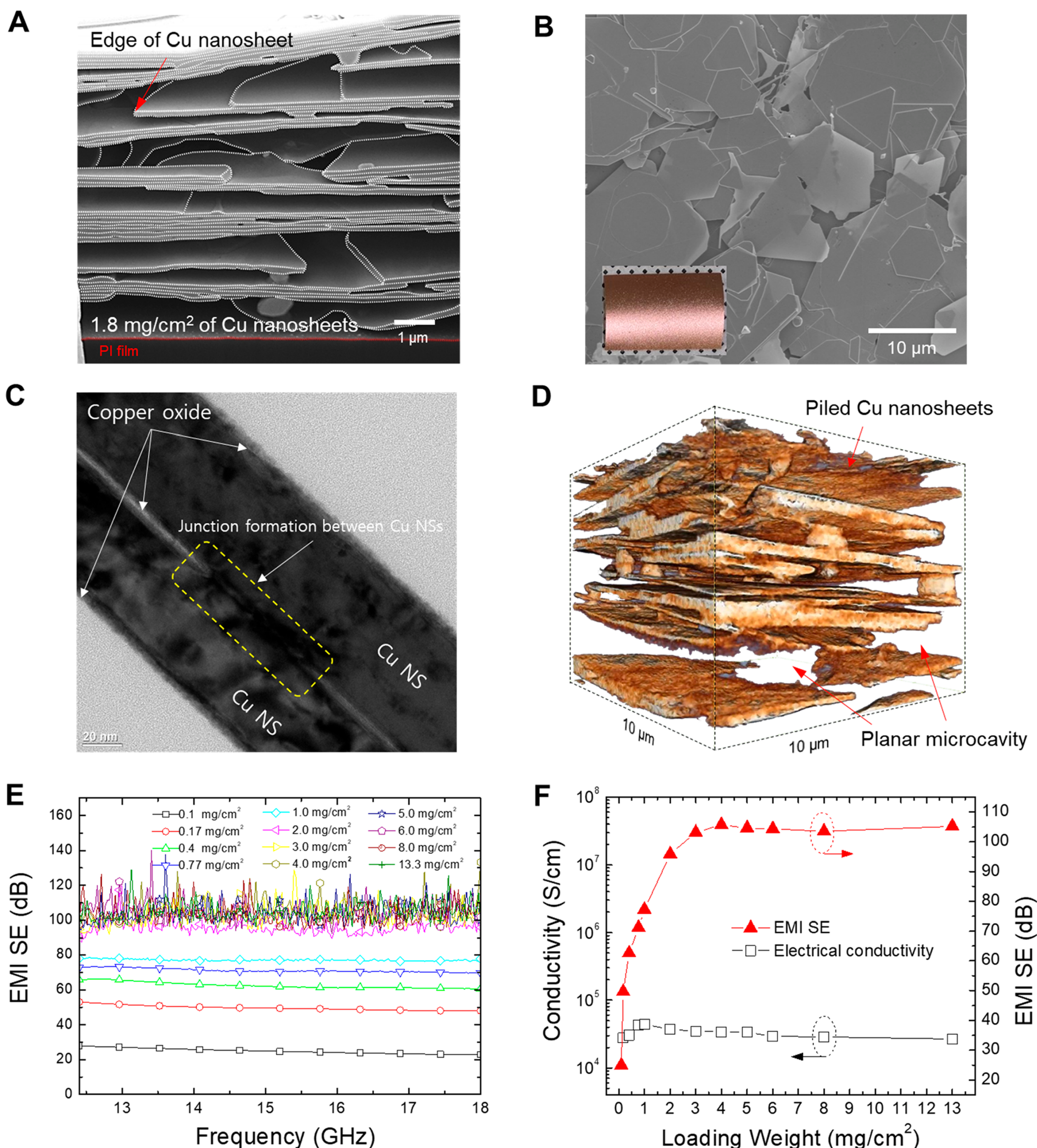

Figure 2. Internal structure and EMI shielding performance of hierarchically structured porous Cu NSs film. (a) Cross-sectional SEM image of a porous Cu film on polyimide substrate with a loading weight of 1.8 mg/cm^2. (b) SEM images of Cu NSs films after H_2/Ar mixture gas annealing. (c) Cross-sectional TEM images of layer-by layer assembled Cu NSs after H_2/Ar mixture gas annealing. (d) 3D XRM image showing piled Cu NSs and sheetlike void (planar microcavity) structures in the middle of the porous film (Movie S1). (e) EMI SE values of the porous Cu films at different loading weights. (f) Electrical conductivity and corresponding EMI SE of the porous Cu NSs films.

monolayered sheets. The basal plane of the Cu NSs corresponds to the (111) plane of the pure copper crystal (clear blue, Figure 1b and Supporting Information, Figure S1). Only 10 Cu nanosheets are needed to cover an area of 10 μm × 10 μm (white dash box), as shown in Figure 1a. Our Cu NSs formed single crystals that grew up to 30 μm in edge length with a thickness of 50−80 nm.[30] Because of their areas and dimensions, these oversized nanoplates are expected to provide good metallic filler materials for forming large-area conductive films over certain substrates. In particular, the Cu NSs are the widest metallic fillers with nanometer-scale thicknesses compared to nanoparticles or nanowires.

https://dx.doi.org/10.1021/acsnano.0c07352
ACS Nano 2021, 15, 829−839

As shown in Figure 1c, the Cu NSs initially adhered to the substrate in a parallel fashion before connecting with neighboring nanoplates during the spray-printing process because of their high edge length (l)-to-thickness (t) aspect ratio. Next, they stacked vertically and side-by-side to establish contacts among them, which produced conductive metallic films. We achieved large area conductive copper films (15 cm × 15 cm) on a polyethylene terephthalate (PET) substrate using a simple spray-printing process as shown in Figure 1d. Interestingly, they showed a very shiny surface similar to that of a commercial dense copper foil, which is atypical of zero- or one-dimensional metallic fillers, such as copper nanoparticles or nanowires. This implies that our Cu NSs are some of the most effective metallic fillers for forming functional conductive films.

As we mentioned above, our Cu NSs have two-dimensional features and resulted in layer-by-layer stacking when they formed a film on a substrate. The internal structure of the film was evaluated by cross-sectional SEM image as shown in Figure 2a. Unlike other conventional thin films or metallic foils, the resulting films had a distinct internal hierarchical structure reminiscent of the geological strata of the Earth. This hierarchical structure presented sheetlike voids (vacant space) between nanosheets, consistent with a random stacking of individual Cu NSs. The void thicknesses measured from tens of nanometers to a few microns. The stacked Cu NSs appeared electrically connected and formed vertical and lateral plane-to-plane contacts with each other.[30] However, because the Cu NSs were completely covered by a very thin native copper oxide phase (Cu_2O) on the basal plane of the Cu NSs during the preparation process, the ultrathin Cu oxide layer acted as a contact barrier (both electrical and mechanical) between the layer-by layer stacked Cu NSs (see Figures S1−S3 in the Supporting Information). Therefore, it required a post annealing process to enhance the electrical contact between Cu NSs that have an oxide phase on the basal plane. In the SEM analysis, we observed a partial melting of Cu NSs at the surface of the film implying a physical connection between the Cu NSs after annealing at 250 °C as shown in Figure 2b (see Figure S4 in the Supporting Information). As a result of annealing, the sheet resistance of Cu NSs film was decreased from 10.07 to 0.059 Ω/□ (see Table S1 in the Supporting Information). For further investigation of the interface interaction between the Cu NSs, we did a high-resolution cross-sectional TEM analysis of the Cu NSs after the annealing process. We clearly observed a physical merging at the interfacial region of Cu NSs, exhibiting the formation of partial junctions between the basal plane of the Cu NSs as shown in Figure 2c (see Figure S5 in the Supporting Information). The junctions become a good conduction path for the current flow between the Cu NSs, reducing the sheet resistance of the Cu NSs film after the annealing process. To verify the internal structure and porosity of the hierarchically structured porous Cu film, we performed nondestructive, high-resolution, three-dimensional X-ray microscope (3D XRM) analyses (Figure 2d). As expected, the porous Cu film kept their hierarchical layer-by-layer structure, exhibiting both piled Cu nanosheets and planar microcavities. The prepared porous Cu film consisted of ∼25%−34% Cu NSs, which resulted in 75%−66% porosity and 2.3−3.0 g/cm^3 film density. These values are in good agreement with the film density calculated using nanosheet loading weights per unit area and the measured film thicknesses.

Considering EMI shielding mechanisms, the hierarchical structures of porous Cu films are expected to strongly affect the EMI shielding capability. Previous studies on EMI shielding materials[9−12] have suggested that the electrical conductivity and internal structure of the shielding film are critical factors for controlling the reflection and absorption of incident electromagnetic waves, respectively. Generally, high electrical conductivity materials, such as metallic films, exhibit high EMI shielding values, because their surface strongly reflects electromagnetic waves.[21] The specific internal architecture of the shielding materials is expected to significantly enhance the SE value by increasing the reflection path of the electromagnetic waves, which dissipates their energy within the film.[1] Consequently, using single-crystalline copper nanosheets and their multilayered architecture is one of the best strategies to achieve extremely high-efficiency EMI SE. To determine the effectiveness of the hierarchically structured porous Cu film as an EMI barrier, 12 kinds of porous Cu films were prepared on a plastic substrate with different loading weights of Cu NSs at unit areas from 0.1 to 13.3 mg/cm^2. We evaluated the EMI SE performance of the resulting film exposed to X-band (8.2−12.4 GHz) and Ku-band frequency ranges (12.4−18 GHz) (see Figure 2e and Figure S6 in the Supporting Information). The samples did not show substantial frequency-dependent EMI SE at the same loading weight (Figure S7 in the Supporting Information). The strong correlation between electrical conductivity and the EMI SE dictates the necessity of formation of a conductive path between each pair of nanosheets. Unlike other metallic filler materials such as nanoparticle or nanowires, Cu NSs are structurally two-dimensional and overlaid to create a so-called electrical plane contact after a thermal annealing process as shown in Figure 2c.

In the early stage of formation of the film, the Cu NSs gradually started to fill the substrate without any conducting paths between them. Therefore, on the one hand, a loading weight of 0.08 mg/cm^2 did not produce any meaningful EMI SE, exhibiting ∼0 dB of EMI SE. On the other hand, higher Cu NSs loadings increased the chance of forming layer-by-layer structure in the as-deposited film. The EMI SE of the Cu NSs followed a trend that was proportional to the loading weight (Figure 2f). Increasing this loading weight dramatically enhanced the EMI SE (Figure 2e,f), which reached a maximum of 100 dB at a loading weight of 3.0 mg/cm^2, corresponding to a film thickness of ∼15 μm. This value, which is the highest EMI SE in this study, implies that the Cu NSs film blocks up to 99.999 999 99% of incident electromagnetic waves. Because of the lower density of the Cu NSs films than that of a dense Cu film or foil, the electrical conductivity of the porous Cu films was much lower than that of conventional copper. It did not show any dependency of the electrical conductivity against the loading weight of Cu NSs, exhibiting an average value of 33 635 S/cm. The highest electronic conductivity (44 444 S/cm) was achieved at a loading weight of 1.0 mg/cm^2 with the thickness of 4.5 μm, as shown in Figure 2f (see Figure S8 and Table S2 in the Supporting Information). Although the electrical conductivity of the Cu NSs film was relatively lower than that of a dense Cu film or foil, it exhibited outstanding EMI SE. The enhanced EMI SE of our Cu NSs films seems to be originated from the internal structure of the porous films. Note that five samples with loading weights exceeding 3.0 mg/cm^2 achieved saturated EMI SE values of

https://dx.doi.org/10.1021/acsnano.0c07352
ACS Nano 2021, 15, 829−839

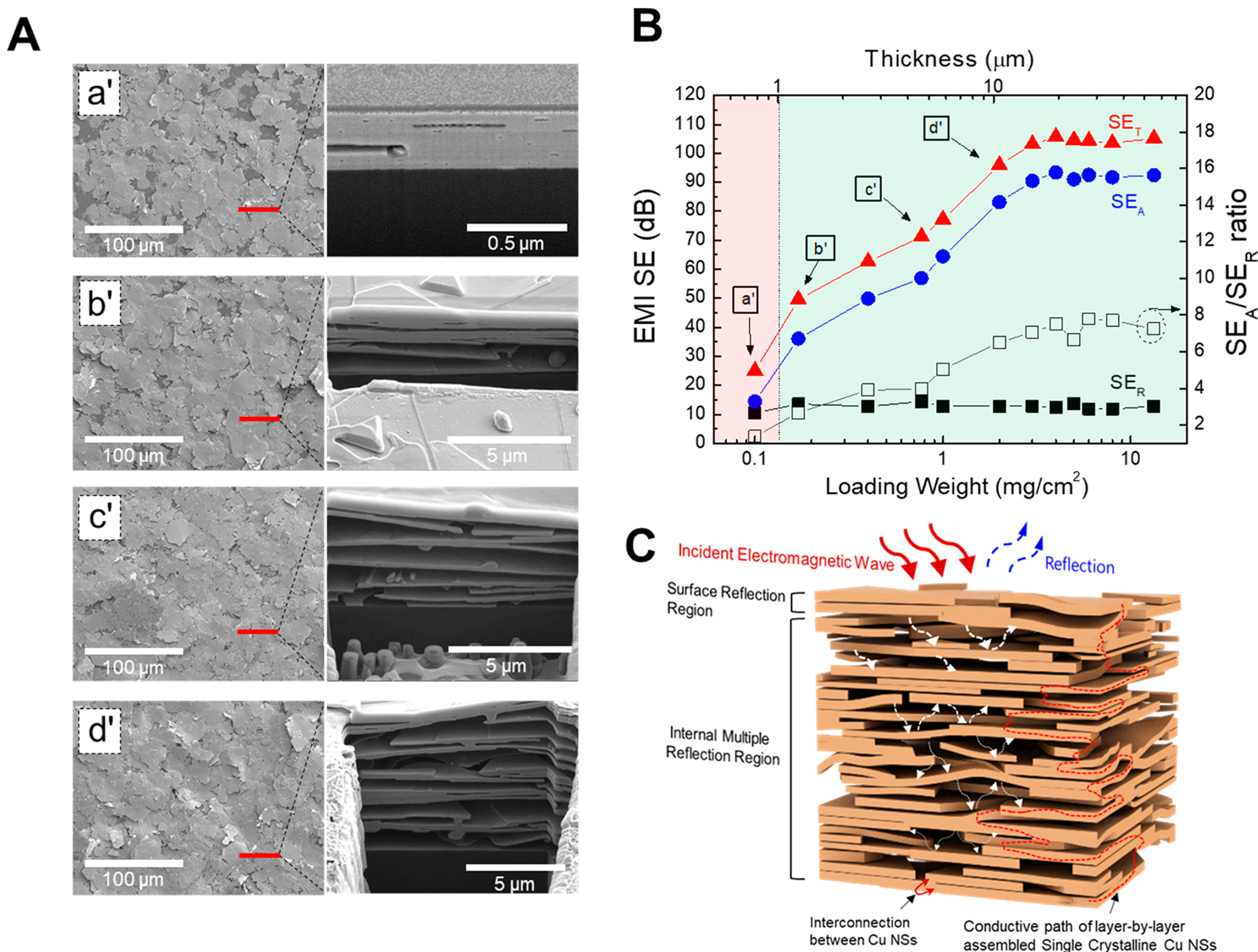

Figure 3. Influence of the internal hierarchical structure of porous Cu films on EMI SE performance. (a) Top-view and cross-sectional SEM images of the porous Cu films with different loading weights of 0.1 (a′), 0.17 (b′), 0.9 (c′), and 1.8 (d′) mg/cm^2. (b) Contribution of absorption (SE_A) and reflection (SE_R) mechanisms on the total EMI SE of porous Cu films. (c) Schematics of the hierarchical porous Cu film and potential EMI shielding mechanism. The incident electromagnetic waves (red arrows) are partly reflected (blue dashed arrows) or absorbed by the porous Cu film surface (white arrows). The absorbed waves (white arrows) meet the multilayered, large-area, single-crystalline 2D Cu NSs in the internal multiple reflection region. In this region, they experience multiple reflections (white arrows) between Cu NSs and lose their energy (thin white arrow) before being extinguished in the Cu NS shielding barrier.

only 105 dB because of limitations in the dynamic measurement range of the network analyzer.

To further investigate the high EMI SE values of the hierarchically structured porous Cu films, we studied the relationship between EMI SE and the internal film architecture as a function of loading weight of the Cu NSs on the substrate (Figure 3). In addition, we carefully analyzed the contribution of the shielding mechanisms to the total shielding effectiveness (SE_T) of our porous Cu films for different internal architectures.

The EMI SE value strongly depends on the electrical conductivity, thickness, and internal structure of the blocking materials.[31] The Cu NSs films were formed using a different process from metallic foils or deposited thin films. We found that the Cu NSs did not completely cover the substrate surface at loading weights lower than 0.1 mg/cm^2 but were partially connected or stacked with each other to form isolated Cu NS islands on the substrate. As a result, we did not identify any electrical conductivity or EMI SE in the film. When the loading weight of the Cu NSs exceeded a certain value (*e.g.*, 0.1 mg/cm^2) (Figure 3b(a′)), more physical connections were observed between neighboring nanosheets, and the sprayed films started to show electrically conductive characteristics. The films exhibited an electrical conduction (R_s) of ∼90 Ω/□ and a measurable EMI SE (SE_T ≈ 25 dB) at 0.1 mg/cm^2 (Figure 3a(a′)). On the one hand, they did not fully cover the substrate, implying that the film was still in the percolation-governed regime (red area, Figure 3a) for EMI shielding. On the other hand, the film obtained at a loading weight of 0.17 mg/cm^2 was completely covered by many Cu NSs and began to form a multilayered internal architecture (Figure 3b(b′)). As loading weight increased above 0.17 mg/cm^2, the films showed better EMI shielding capability, with an SE_T value of 49.6 dB. The absorption mechanism (SE_A = 36.1 dB) contributed to EMI shielding to a greater extent than its reflection counterpart (SE_R = 13.5 dB). In the higher loading weight regime, the multilayered internal structure was expanded by covering each Cu NS. These contributions were proportional to the loading weight of the Cu NSs (Figure 3b(c′, d′)). This loading-weight dependence clearly demon-

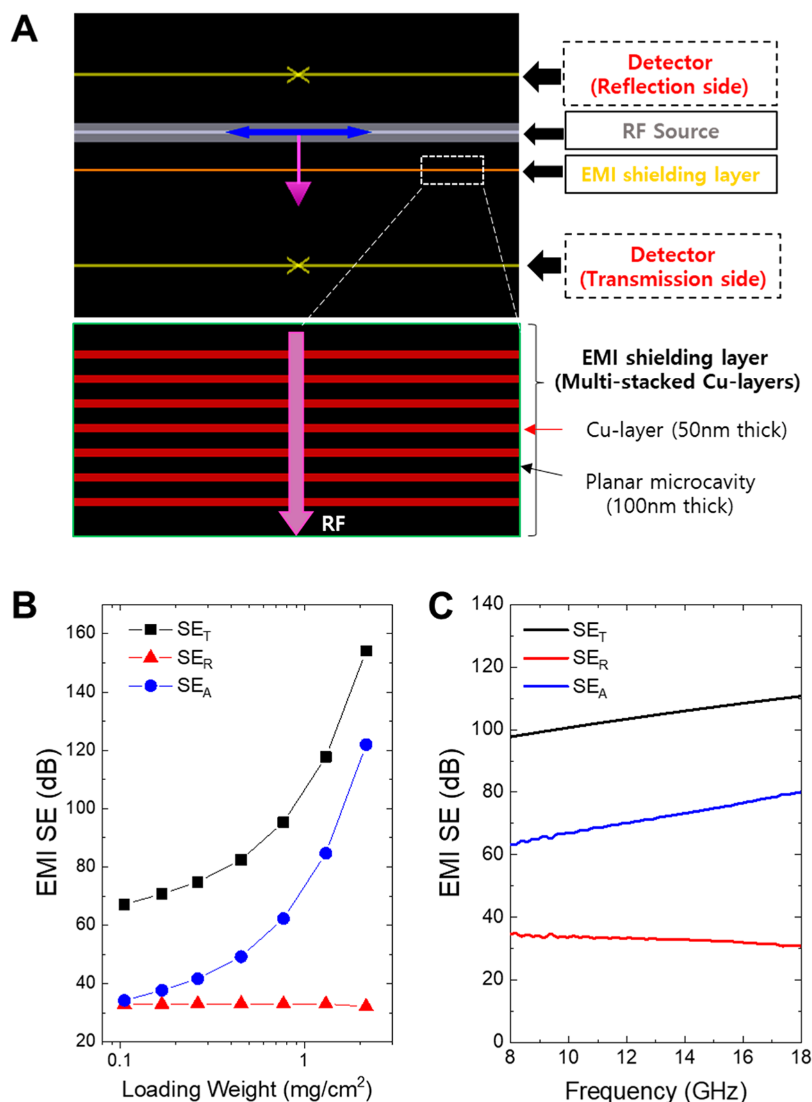

Figure 4. FDTD simulation of the effects of multilayered architecture on EMI SE_T, SE_A, and SE_R. (a) Schematics of the multistacked Cu layers. (b) Calculated EMI SE values of the multilayered EMI shielding model at different loading weights. The contribution of the absorption mechanism to SE_T is considerable at high loading weights, implying the effectiveness of the multilayered architecture on EMI shielding. (c) Calculated EMI SE values of the multilayered structure at a loading weight of 1.0 mg/cm^2 for frequencies ranging from 8.0 to 18.0 GHz.

strated that the internal structure governs the EMI SE (SE_T) of the Cu NSs. Interestingly, the calculated SE_R values of the films were independent of the loading weight and ranged between 10 and 14 dB for loading weights spanning from 0.1 to 13.3 mg/cm^2. This result implies that the internal structure of the films is strongly related to the absorption mechanism. In addition, the hierarchically structured porous Cu film had a critical boundary condition that depends on the loading weight (~0.15 mg/cm^2) between the percolation- (red) and architecture-governed regimes (green area, Figure 3a). On the one hand, in the percolation-governed regime, which involves both reflection and absorption mechanisms, the SE_A/SE_R ratio was ~1.4 (Figure 3a(a′)). On the other hand, the absorption mechanism became predominant in the architecture-governed regime (over 0.17 mg/cm^2 of Cu NSs), resulting in increased SE_A/SE_R ratio to ~7.5.

These unexpectedly high EMI SE values (~100 dB at a loading weight of 3.0 mg/cm^2 corresponding to a film thickness of 15 μm) seem to originate from the structural specificity of porous Cu film. This is attributed to the single crystallinity of the nanosheets, which allows homogeneous electrical conductivity, and their 2D geometry, which leads to the formation of electrical plane contacts and the internal hierarchical structure. Figure 3c shows schematics of the porous Cu film and its internal hierarchical structure. In general, electromagnetic waves are reflected at an interface between materials with a large difference in impedance. A similar phenomenon can occur at the surface of single-crystalline Cu nanosheets that simultaneously display physical and electrical plane contacts. Because of the repeated stacking of the Cu NSs, the porous Cu films exhibited similar micro/nanostructured surfaces and internal hierarchical structures regardless of loading weight, unlike conventional dense copper foils or thin films, which have very smooth surfaces and homogeneously dense internal film structures. The internal hierarchical structure, which is the main feature of our porous Cu films, controls EMI SE. Consequently, the contribution of surface reflection appeared limited and resulted in saturated

https://dx.doi.org/10.1021/acsnano.0c07352
ACS Nano 2021, 15, 829−839

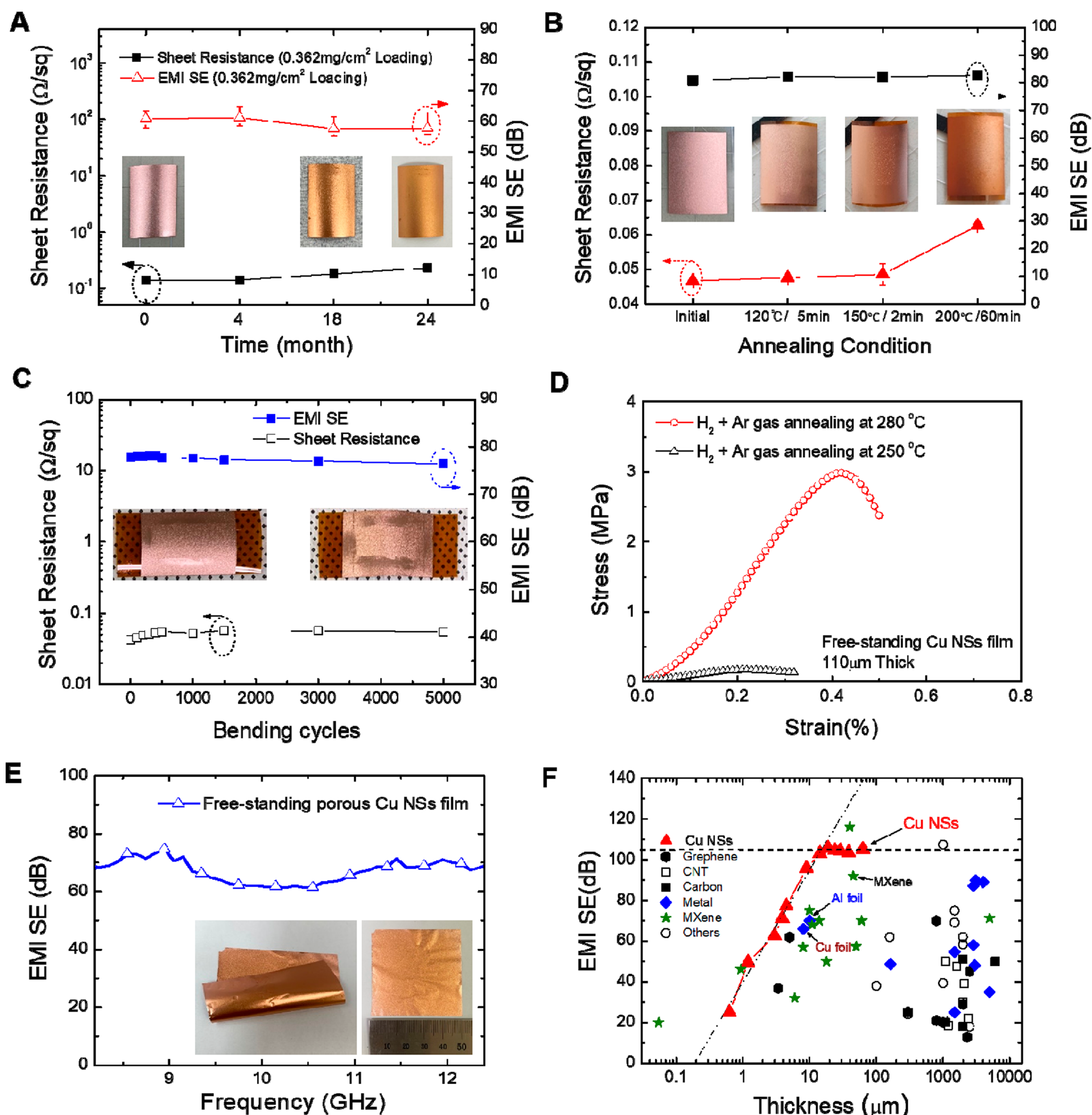

Figure 5. Reliability of the hierarchical porous Cu NSs film and performance comparisons of shielding materials. (a) Long-term stability of EMI SE and sheet resistance of the Cu NSs film. (b) Durability of the Cu NSs film with a loading weight of Cu NSs of ∼1.0 mg/cm^2 at various ambient annealing conditions. (c) EMI SE and sheet resistance of Cu NSs film with a loading weight of Cu NSs of ∼1.0 mg/cm^2 at repeated bending cycles. (d) Typical stress−strain curves of the free-standing Cu NSs films with thickness of 110 μm. (e) EMI SE performance of 5 μm thick, free-standing, porous Cu NSs film (5 cm × 5 cm). (f) EMI SE values of reported materials as a function of film thickness (Table S4 for more information). The black dashed line above 100 dB is a limitation of the dynamic range of the network analyzer. The red dotted line is an extrapolation of the expected EMI SE of the hierarchical porous Cu NSs films.

EMI SE_R values. The interaction of incident electromagnetic waves with a laminated internal structure strongly affected the ultimate shielding performance of our porous Cu film. In contrast with existing solution-processable, conductive metal-based EMI shielding materials, our single-crystalline Cu NSs retained their hierarchical structure and formed an effective conductive path by electrical plane contacts that facilitated electron mobility throughout the films. These structural features gave rise to very long travel paths for incident electromagnetic waves, which consequently lose their energy by scattering between the Cu NSs; they are ultimately eliminated in the porous Cu film by transforming into heat.[13,19,32] These phenomena are responsible for multiple electromagnetic reflections or resonances between individual Cu NSs, resulting in an extremely strong absorption mechanism contribution to EMI shielding and the high SE_T

https://dx.doi.org/10.1021/acsnano.0c07352
ACS Nano 2021, 15, 829−839

value of the porous Cu NSs films (Figure 3b). On the one hand, the contribution of SE_A at a hierarchical structure on EMI SE_T is expected to increase from 34 to 70 dB after the loading weight is increased from 0.1 to 1.0 mg/cm^2. On the other hand, the effect of the SE_R on EMI SE_T was independent of loading weight changes.

To verify the validity of the hierarchical structure on the EMI SE, we performed additional FDTD numerical simulations as shown in Figure 4. Because the Cu NSs were substantially thinner (a few microns) than the RF wavelengths of interest (a few millimeters), the simulation domain needed to be meshed (discretized) into a number of points. Consequently, the simulation was performed in the 2D domain, instead of 3D, so that it could be completed within a reasonable amount of time. The 2D domain consisted of a radio frequency (RF) source (gray, 8−18 GHz), shielding structure (orange), and two detectors (red) at reflection and transmission sides, which were all assumed to be infinitely long in the horizontal direction (Figure 4a). The source generated RF planar waves that traveled perpendicular to the shielding structure (along the magenta arrow) and were linearly polarized in the direction parallel to the shielding structure (blue arrow). Because the 2D simulation assumed that the objects designed in the 2D plane extended infinitely into the screen, rotation of polarization around the wave propagation did not change the simulation results. This is also the case for randomly polarized waves. Once the RF wave emerged from the source and interacted with the shielding structure, a portion of the input power was absorbed by the shielding material, while the rest was either reflected or transmitted, which was measured by two detectors.

The 3D XRM analysis of our experimentally fabricated hierarchically structured porous Cu film yielded a volume fraction of ∼33.3% for copper. Thus, the FDTD simulation was performed at the ideal layer-by-layer structure (stack of 50 nm thick Cu thin film with a 100 nm thick airgap spacing in between), and the electric conductivity of each Cu-nanosheet was set to be 6×10^7 S/m, which is the identical value of pure Cu. The number of layers, which is directly proportional to the thickness of the structure, was converted to the loading weight using the thickness−loading weight relation obtained in Figure 4b.

The FDTD simulation estimated SE_T, SE_R, and SE_A values using Equations 1, (2), and (3) (see the Supporting Information) and the measured reflectance and transmittance for different loading weights.

$$SE_T = SE_R + SE_A \quad (1)$$

$$SE_R = 10\log\left(\frac{1}{1-R}\right) = 10\log\left(\frac{1}{1-|\underline{S}_{11}|^2}\right) \quad (2)$$

$$SE_A = 10\log\left(\frac{1}{1-A_{\text{eff}}}\right) = 10\log\left(\frac{1-R}{T}\right) = 10\log\left(\frac{1-|\underline{S}_{11}|^2}{|\underline{S}_{21}|^2}\right) \quad (3)$$

First, the simulation was used to analyze the EMI shielding of Cu NSs with a loading weight of 1.0 mg/cm^2, and the result is shown in Figure 4c in the frequency domain. The obtained SE spectra were nearly linear in a wide frequency range of 8−18 GHz, confirming that the mean value of the entire frequency range could be used for further comparison of the SE values estimated for different loading weights. Figure 4b shows that further stacking of Cu NSs increased the overall shielding effectiveness (SE_T), and most of this enhancement originates from the increased absorption (SE_A), while the reflection (SE_R) of the thicker structure remained almost the same. The highly enhanced absorption-related SE in the multilayered structure was mainly attributed to multireflection, where the incoming RF signal was captured inside the volume and increased the propagation path of the trapped wave bouncing back and forth (while experiencing absorption). Multireflection, which provides different phase shifts for different propagation paths throughout the shield, causes the original planar wavefront to lose its phase coherence, and this phase mismatching behaves like another absorption mechanism. There is some variation between the calculated EMI SE values and the experimental results using Cu NSs films, but both results show very similar EMI shielding behavior, indicating improved shielding with respect to layer-by-layer structure formation. It seems to be due to the difference between the boundary conditions (structure and conductivity) of the calculation and the experimental results. The boundary conditions of the calculations (perfect periodic structure and high electrical conductivity) are ideal compared to real Cu NSs films with randomly staked structures and low electrical conductivity. Therefore, we believe that the FDTD calculation is valid to account for the contribution of layer-by-layer assembly of metal sheets to the improved EMI shielding efficiency.[1,22,35] This implies that our porous Cu films are appealing substitutes for conventional metallic EMI shielding films, such as Al or Cu foil.

For further practical EMI shielding applications, we performed reliability tests of the hierarchically structured porous Cu NSs film (such as long-term, temperature, bending, and mechanical strength tests) without a protecting layer over the film. We carefully prepared a porous Cu film with a loading weight of 0.362 mg/cm^2 on a polyimide (PI) substrate and monitored its sheet resistance and EMI SE with respect to time at room temperature, as shown in Figure 5a. The pristine, porous Cu film clearly showed a pure copper color and ∼0.15 Ω/□ and ∼60 dB sheet resistance and EMI SE, respectively. The stability of the porous Cu film was maintained for four months under ambient conditions without any additional protecting layers, exhibiting negligible changes in both sheet resistance and EMI SE performance. As mentioned above, our porous Cu film was organized by layer-by-layer stacking of individual single-crystalline copper nanosheets with a (111) basal plane. It is known that the (111) surface of copper is likely to form hexagonal structures with adsorbed oxygen, and that structure acts as the initial layer of Cu_2O, which is considered a good template layer for further growth of thicker layers.[33] In addition, it seems that the initial Cu_2O layer on the basal plane of the Cu nanosheet effectively reduced the oxidation rate, because the Cu_2O crystal reduced the path for mass transportation.[34] Similarly, we clearly observed very thin (less than 5 nm thick) and dense Cu_2O layer on the basal plane(111) of the Cu NSs from both a phase image of EBSD and a cross-sectional TEM analysis (see Figures S1 and S3 in the Supporting Information). The Cu_2O layer on the Cu NSs may enable the possibility of an extraordinary stability of the porous Cu NSs film against further oxidation under ambient condition. Thus, even though the sample was stored under ambient conditions for almost 24 months, we observed little

https://dx.doi.org/10.1021/acsnano.0c07352
ACS Nano 2021, 15, 829−839

degradation of the shielding properties compared to the pristine state except for a minor change in color (brown) and an increase in sheet resistance up to 0.2 Ω/□. This means that the porous Cu film retained its hierarchical structure and conductive core in the Cu nanosheets. The unexpected stability of our porous Cu film may be due to the structural properties of the single-crystalline copper nanosheet. We also investigated the durability of the porous Cu film with a loading weight of Cu NSs of ~1.0 mg/cm^2 at various annealing conditions, as shown in Figure 5b. The sheet resistance of the film increased in a manner proportional to temperature, indicative of surface oxidation of the single-crystalline Cu NSs with a change in color from pink (pristine porous Cu film) to brown. Nevertheless, the EMI SE performance was well-maintained, exhibiting almost 80 dB without any degradation after a 200 °C annealing under atmosphere for 1 h.

To verify the flexibility and electrical stability of the porous Cu NSs film, the EMI SE and sheet resistance of the films were monitored for up to 5000 bending cycles, as shown in Figure 5c.[36−38] The loading weight of Cu NSs was fixed at 1.0 mg/cm^2 on the PI (4 cm × 2 cm), and the deposited area was 3 cm × 2 cm. The sheet resistance and EMI SE of the Cu NSs film was 0.0126 Ω/□ and 77.75 dB, respectively. The Cu NSs films maintains well their sheet resistance and EMI SE value after 5000 cycles of bending (bending radius ≈ 2.75 mm), which indicates the robustness and excellent flexibility of our Cu NSs films against a repeated bending condition. In particular, we found negligible differences in the morphology of the Cu NSs film without any significant delamination or deformation in both pristine and a bending test of 5000 cycles (see Figures S9 and S10 and Table S3 in the Supporting Information). To investigate the mechanical property of Cu NSs film as shown in Figure 5d, we introduced the mechanical exfoliating method to prepare free-standing porous Cu NSs film. Compared to other metal thin films composed of zero- or one-dimensional metal nanocrystals, our porous Cu film has a distinct hierarchical structure based on a layer-by-layer assembly of Cu NSs, resulting in planar contact. Because the forming gas-annealing process allows better physical planar contact between Cu NSs (Figure 2b,c) by merging at the interface between each Cu NS, the Cu NSs film maintained its free-standing film shape during and after the exfoliation process. The sample dimensions of the free-standing Cu NSs film for testing was the length, width, and thickness of 20 mm, 1 mm, and 110 μm, respectively. From the stress−strain curves as shown in Figure 5d, the tensile strength was 0.12 ± 0.06 and 2.24 ± 0.8 MPa, and the elastic modulus was 74.5 ± 19.8 and 634.7 ± 164.6 MPa for 250 and 280 °C annealing, respectively. As we discussed above, we found a physical coalescence at the interfacial region of the Cu NSs, indicating a formation of partial junctions between the basal plane of the Cu NSs. If partial junctions are formed in the interfacial region of Cu NS after annealing, the number of mechanical contacts increases, which can improve the mechanical strength of the Cu NSs film. We expect more physical merging at the interfacial region of Cu NSs formed at a higher annealing temperature. Therefore, the free-standing Cu NSs film with a higher annealing temperature showed superior mechanical properties than that of a lower condition. However, the mechanical properties of our free-standing Cu NSs film was much lower than that of conventional dense copper foil due to its porous structure with layer-by-layer assembly. We also measured the EMI SE performance on the prepared free-standing porous Cu NSs film with resulting size and thickness of 5 cm × 5 cm and ~5 μm, respectively. The free-standing porous Cu NSs film looked like a commercially available high-density copper foil with a very glossy surface as shown in Figure 5e. It also showed excellent EMI SE performance with an average 65 dB in the X-band frequency range. This outstanding EMI shielding performance can be achieved at thicknesses of the 10 μm commercialized copper foil, which demonstrates the efficiency of our hierarchically structured porous Cu NSs film (see Figure S11 in the Supporting Information).

On the basis of the above experimental results, porous Cu NSs films with hierarchical internal structures are expected to be one of the most lightweight and cost-efficient solution-processable shielding materials. A literature survey of the shielding effectiveness of several known materials (MXene, CNT, graphene, Cu or Al foils, *etc.*) revealed that our porous Cu NSs films are the best EMI shielding materials currently (Figure 5f). In particular, the films displayed the best EMI SE (closed red triangle) over the assessed thickness range (~15 μm), even relative to other thicker materials. The extrapolation (red dotted line) suggests that porous Cu NSs films thicker than 15 μm can outperform existing thicker films (Figure 5f). They also showed an extremely high specific EMI SE value (SSE/t = 292 000 dB·cm^2/g at 1.6 μm thick) compared to conventional high-performance materials and emerging atomically thin 2D materials, such as graphene, graphene oxide, and MXene (Figure S12 and Table S4 in the Supporting Information), at practically applicable thickness ranges. These results suggest that hierarchically structured porous Cu NSs films are promising candidates for potential use in common commercial and extremely high-level EMI shielding applications.

CONCLUSIONS

Large-area, two-dimensional, single-crystalline Cu NSs were proposed as conductive fillers for EMI shielding applications. Because of its structure, the hierarchical porous Cu NSs film exhibited a particularly high EMI SE performance over a wide range of thicknesses, outperforming any known synthetic materials. The internal layer-by-layer stacking of Cu NSs and their interactions with incident electromagnetic waves are responsible for the strong absorption of this radiation. The exceptional EMI shielding efficiency and cost-effectiveness of the porous Cu films will make them essential components of commercial products as next-generation shielding barriers. We believe that our research represents an important practical approach for using metallic 2D nanocrystals. These large-area 2D metallic nanocrystals will serve as conductive fillers for enhancing performance in a wide range of electronics applications.

EXPERIMENTAL SECTION

Preparation of Porous Cu NSs Film. The Cu NSs were synthesized by a conventional hydrothermal method.[30] Copper(II) chloride dihydrate ($CuCl_2{\cdot}2H_2O$, 99+%), hexadecylamine (HDA, 98%), glucose (99.5+%), and iodine (I_2, 99.8+%) were purchased from Sigma-Aldrich. The polyimide film (thickness: 75 μm) was purchased from MINSUNG EIM. To prepare a hierarchical porous Cu film, Cu NSs were carefully mixed in chloroform at a concentration of 1 mg/mL. The mixture solutions were spray-painted onto a polyimide substrate (2.5 cm × 2.5 cm) using a commercially available hand-held air bush (Harder & Steenbeck). The prepared Cu NSs film were dried on a hot plate at 70 °C for 5 min. The samples were annealed at 250 °C for 1 h in a tube furnace under a flowing

https://dx.doi.org/10.1021/acsnano.0c07352
ACS Nano 2021, 15, 829−839

forming gas (5:95 H_2/Ar gas mixture). The free-standing Cu NSs film was prepared in the same manner as the porous Cu NSs film. The free-standing film was carefully exfoliated from the silicon oxide substrate. For comparison, copper thin films were evaporated on the polyimide films at a deposition rate of 1.0 Å/s using a thermal evaporator under a pressure of 2×10^{-7} Torr.

Characterization of Porous Cu NSs Film. The morphology of the hierarchical porous Cu NSs film was determined by field emission scanning electron microscopy (FESEM) (Nova, FEI, and SU70, HITACHI). Cross-sectional SEM imaging and EBSD analyses were performed by focused ion beam scanning electron microscopy (Helios NanoLab 650, FEI company). Cross-sectional TEM imaging analyses were performed by using Cs-Corrected Scanning Transmission Electron Micros (JEM-ARM200F, JEOL).

Nondestructive 3D structural analysis was performed using a 3D X-ray Tomography Microscope System (Xradia Ultra, Zeiss). The sheet resistance of the Cu NS film was measured using a four-point probe resistance measurement system (FPP RS-8 and Arms-600, Dasol ENG). The EMI SE measurements for X-band (8−12 GHz) and Ku-band (12−18 GHz) ranges were performed using WR-90 and WR-62 coaxial-type rectangular waveguide fixtures (Agilent Technologies, X281A and P281B Coaxial Waveguide Adapter), respectively, with two kinds of two-port network analyzers (Agilent/HP 8720C 50 MHz−20 GHz and E5071C 300 kHz−20 GHz). The incident power of the electromagnetic wave was 1 mW, which was set as 0 dBm. The samples were carefully and tightly fixed with screws to avoid undesired leakage of electromagnetic waves. The WR-90 (8.2 to 12.4 GHz) and WR-62 (12.4 to 18 GHz) test fixtures required samples with inner dimensions of 22.86 mm (W) × 10.19 mm (H) and 15.80 mm (W) × 7.90 mm (H), respectively. The bending test was performed by a homemade bending machine. The mechanical property of the free-standing Cu NSs film was evaluated using a FAVIMAT+ machine (Textechno).

ASSOCIATED CONTENT

Supporting Information

The Supporting Information is available free of charge at https://pubs.acs.org/doi/10.1021/acsnano.0c07352.

Calculation of EMI SE of the porous Cu NS films, SEM, EBSD, cross-sectional TEM, electrical conductivity and EMI SE (PDF)

XRM analysis of porous Cu film with Cu NSs (AVI)

AUTHOR INFORMATION

Corresponding Author

Tae-Wook Kim − *Department of Flexible and Printable Electronics, LANL-CBNU Engineering Institute-Korea, Jeonbuk National University, Jeonju 54896, Republic of Korea;* orcid.org/0000-0003-2157-732X; Email: twk@jbnu.ac.kr

Authors

Ho Kwang Choi − *Department of Flexible and Printable Electronics, LANL-CBNU Engineering Institute-Korea, Jeonbuk National University, Jeonju 54896, Republic of Korea*

Aram Lee − *Functional Composite Materials Research Center, Institute of Advanced Composite Materials, Korea Institute of Science and Technology, Jeollabuk-do 55324, Republic of Korea*

Mina Park − *Functional Composite Materials Research Center, Institute of Advanced Composite Materials, Korea Institute of Science and Technology, Jeollabuk-do 55324, Republic of Korea*

Dong Su Lee − *Functional Composite Materials Research Center, Institute of Advanced Composite Materials, Korea Institute of Science and Technology, Jeollabuk-do 55324, Republic of Korea;* orcid.org/0000-0003-2456-0646

Sukang Bae − *Functional Composite Materials Research Center, Institute of Advanced Composite Materials, Korea Institute of Science and Technology, Jeollabuk-do 55324, Republic of Korea;* orcid.org/0000-0002-3019-0584

Seoung-Ki Lee − *Functional Composite Materials Research Center, Institute of Advanced Composite Materials, Korea Institute of Science and Technology, Jeollabuk-do 55324, Republic of Korea;* orcid.org/0000-0002-8786-0251

Sang Hyun Lee − *School of Chemical Engineering, Chonnam National University, Gwangju 61186, Republic of Korea;* orcid.org/0000-0002-7784-5939

Takhee Lee − *Department of Physics and Astronomy, and Institute of Applied Physics, Seoul National University, Seoul 08826, Republic of Korea;* orcid.org/0000-0001-5988-5219

Complete contact information is available at: https://pubs.acs.org/10.1021/acsnano.0c07352

Notes

The authors declare no competing financial interest.

ACKNOWLEDGMENTS

This work was supported by the National Research Foundation of Korea (2020R1A2C2010163) and partially supported by the Korea Institute of Science and Technology Institutional Program and Korea Institute for Advancement of Technology grant funded by the Korea Government (MOTIE) (P0002007). T.L. is thankful for the financial support of the National Creative Research Laboratory program (Grant No. 2012026372). The authors thank Dr. J.-M. Koo for helping with the EMI SE measurements.

REFERENCES

(1) Shahzad, F.; Alhabeb, M.; Hatter, C. B.; Anasori, B.; Man Hong, S.; Koo, C. M.; Gogotsi, Y. Electromagnetic Interference Shielding with 2D Transition Metal Carbides (MXenes). *Science* **2016**, *353*, 1137−1140.

(2) Chen, Z.; Xu, C.; Ma, C.; Ren, W.; Cheng, H. M. Lightweight and Flexible Graphene Foam Composites for High-Performance Electromagnetic Interference Shielding. *Adv. Mater.* **2013**, *25*, 1296−1300.

(3) Liu, J.; Zhang, H. B.; Sun, R.; Liu, Y.; Liu, Z.; Zhou, A.; Yu, Z. Z. Hydrophobic, Flexible, and Lightweight MXene Foams for High-Performance Electromagnetic-Interference Shielding. *Adv. Mater.* **2017**, *29*, 1702367.

(4) Yang, Y.; Gupta, M. C.; Dudley, K. L.; Lawrence, R. W. Novel Carbon Nanotube- Polystyrene Foam Composites for Electromagnetic Interference Shielding. *Nano Lett.* **2005**, *5*, 2131−2134.

(5) Saini, P.; Choudhary, V.; Singh, B. P.; Mathur, R. B.; Dhawan, S. K. Polyaniline-MWCNT Nanocomposites for Microwave Absorption and EMI Shielding. *Mater. Chem. Phys.* **2009**, *113*, 919−926.

(6) Chung, D. D. L. Materials for Electromagnetic Interference Shielding. *J. Mater. Eng. Perform.* **2000**, *9*, 350−354.

(7) Zhang, Y.; Huang, Y.; Zhang, T.; Chang, H.; Xiao, P.; Chen, H.; Huang, Z.; Chen, Y. Broadband and Tunable High-Performance Microwave Absorption of an Ultralight and Highly Compressible Graphene Foam. *Adv. Mater.* **2015**, *27*, 2049−2053.

(8) Wang, L.; Huang, Y.; Sun, X.; Huang, H.; Liu, P.; Zong, M.; Wang, Y. Synthesis and Microwave Absorption Enhancement of Graphene@Fe_3O_4@SiO_2@NiO Nanosheet Hierarchical Structures. *Nanoscale* **2014**, *6*, 3157−3164.

(9) Chung, D. D. L. Electromagnetic Interference Shielding Effectiveness of Carbon Materials. *Carbon* **2001**, *39*, 279−285.

(10) Das, N. C.; Liu, Y.; Yang, K.; Peng, W.; Maiti, S.; Wang, H. Single-Walled Carbon Nanotube/Poly (methyl Methacrylate) Composites for Electromagnetic Interference Shielding. *Polym. Eng. Sci.* **2009**, *49*, 1627−1634.
(11) Geetha, S.; Satheesh Kumar, K. K.; Rao, C. R.; Vijayan, M.; Trivedi, D. C. EMI Shielding: Methods and Materials—A Review. *J. Appl. Polym. Sci.* **2009**, *112*, 2073−2086.
(12) Kaiser, K. L. *Electromagnetic Shielding;* Taylor and Francis: New York, 2005; pp 1−52.
(13) Al-Saleh, M. H.; Saadeh, W. H.; Sundararaj, U. EMI Shielding Effectiveness of Carbon Based Nanostructured Polymeric Materials: A Comparative Study. *Carbon* **2013**, *60*, 146−156.
(14) Al-Saleh, M. H.; Sundararaj, U. Electromagnetic Interference Shielding Mechanisms of CNT/Polymer Composites. *Carbon* **2009**, *47*, 1738−1746.
(15) Cao, M. S.; Wang, X. X.; Cao, W. Q.; Yuan, J. Ultrathin Graphene: Electrical Properties and Highly Efficient Electromagnetic Interference Shielding. *J. Mater. Chem. C* **2015**, *3*, 6589−6599.
(16) Agnihotri, N.; Chakrabarti, K.; De, A. Highly Efficient Electromagnetic Interference Shielding Using Graphite Nanoplatelet/Poly (3, 4-Ethylenedioxythiophene)-Poly (styrenesulfonate) Composites with Enhanced Thermal Conductivity. *RSC Adv.* **2015**, *5*, 43765−43771.
(17) Li, Y.; Pei, X.; Shen, B.; Zhai, W.; Zhang, L.; Zheng, W. Polyimide/Graphene Composite Foam Sheets with Ultrahigh Thermostability for Electromagnetic Interference Shielding. *RSC Adv.* **2015**, *5*, 24342−24351.
(18) Shen, B.; Zhai, W.; Zheng, W. Ultrathin Flexible Graphene Film: An Excellent Thermal Conducting Material with Efficient EMI Shielding. *Adv. Funct. Mater.* **2014**, *24*, 4542−4548.
(19) Zhang, H. B.; Yan, Q.; Zheng, W. G.; He, Z.; Yu, Z. Z. Tough Graphene- Polymer Microcellular Foams for Electromagnetic Interference Shielding. *ACS Appl. Mater. Interfaces* **2011**, *3*, 918−924.
(20) Fugetsu, B.; Sano, E.; Sunada, M.; Sambongi, Y.; Shibuya, T.; Wang, X.; Hiraki, T. Electrical Conductivity and Electromagnetic Interference Shielding Efficiency of Carbon Nanotube/Cellulose Composite Paper. *Carbon* **2008**, *46*, 1256−1258.
(21) Thomassin, J. M.; Jerome, C.; Pardoen, T.; Bailly, C.; Huynen, I.; Detrembleur, C. Polymer/Carbon Based Composites as Electromagnetic Interference (EMI) Shielding Materials. *Mater. Sci. Eng., R* **2013**, *74*, 211−232.
(22) Wan, S.; Chen, Y.; Wang, Y.; Li, G.; Wang, G.; Liu, L.; Zhang, J.; Liu, Y.; Xu, Z.; Tomsia, A. P.; Jiang, L.; Cheng, Q. Ultrastrong Graphene Films *via* Long-Chain π-Bridging. *Matter.* **2019**, *1*, 389−401.
(23) Li, W.; Qiu, T.; Wang, L.; Ren, S.; Zhang, J.; He, L.; Li, X. Preparation and Electromagnetic Properties of Core/Shell Polystyrene@ Polypyrrole@ Nickel Composite Microspheres. *ACS Appl. Mater. Interfaces* **2013**, *5*, 883−891.
(24) Zhang, H.; Zhang, J. Lightweight Silver@ Carbon Microsphere@ Graphene (Ag@ CMS@ GR) Composite Materials for Highly Efficiency Electromagnetic Interference Shielding Properties. *J. Appl. Polym. Sci.* **2020**, *137*, 48459.
(25) Panigrahi, R.; Srivastava, S. K. Trapping of Microwave Radiation in Hollow Polypyrrole Microsphere through Enhanced Internal Reflection: A Novel Approach. *Sci. Rep.* **2015**, *5*, 7638.
(26) Yang, X.; Fan, S.; Li, Y.; Guo, Y.; Li, Y.; Ruan, K.; Zhang, S.; Zhang, J.; Kong, J.; Gu, J. Synchronously Improved Electromagnetic Interference Shielding and Thermal Conductivity for Epoxy Nanocomposites by Constructing 3D Copper Nanowires/Thermally Annealed Graphene Aerogel Framework. *Composites, Part A* **2020**, *128*, 105670.
(27) Zhao, H.; Hou, L.; Bi, S.; Lu, Y. Enhanced X-Band Electromagnetic-Interference Shielding Performance of Layer-Structured Fabric-Supported Polyaniline/Cobalt-Nickel Coatings. *ACS Appl. Mater. Interfaces* **2017**, *9*, 33059−33070.
(28) Ma, J.; Zhan, M.; Wang, K. Ultralightweight Silver Nanowires Hybrid Polyimide Composite Foams for High-Performance Electromagnetic Interference Shielding. *ACS Appl. Mater. Interfaces* **2015**, *7*, 563−576.
(29) Xu, Y.; Li, Y.; Hua, W.; Zhang, A.; Bao, J. Light-Weight Silver Plating Foam and Carbon Nanotube Hybridized Epoxy Composite Foams with Exceptional Conductivity and Electromagnetic Shielding Property. *ACS Appl. Mater. Interfaces* **2016**, *8*, 24131−24142.
(30) Lee, J. W.; Han, J.; Lee, D. S.; Bae, S.; Lee, S. H.; Lee, S. K.; Moon, B. J.; Choi, C.-J.; Wang, G.; Kim, T. W. 2D Single-Crystalline Copper Nanoplates as a Conductive Filler for Electronic Ink Applications. *Small* **2018**, *14*, 1703312.
(31) Simon, R. M. EMI Shielding through Conductive Plastics. *Polym.-Plast. Technol. Eng.* **1981**, *17*, 1−10.
(32) Ameli, A.; Nofar, M.; Wang, S.; Park, C. B. Lightweight Polypropylene/Stainless-Steel Fiber Composite Foams with Low Percolation for Efficient Electromagnetic Interference Shielding. *ACS Appl. Mater. Interfaces* **2014**, *6*, 11091−11100.
(33) Gattinoni, C.; Michaelides, A. Atomistic Details of Oxide Surfaces and Surface Oxidation: The Example of Copper and Its Oxides. *Surf. Sci. Rep.* **2015**, *70*, 424−447.
(34) Lee, S. K.; Hsu, H. C.; Tuan, W. H. Oxidation Behavior of Copper at a Temperature below 300 °C and the Methodology for Passivation. *Mater. Res.* **2016**, *19*, 51−56.
(35) Iqbal, A.; Shahzad, F.; Hantanasirisakul, K.; Kim, M. K.; Kwon, J.; Hong, J.; Kim, H.; Kim, D.; Gogotsi, Y.; Koo, C. M. Anomalous Absorption of Electromagnetic Waves by 2D Transition Metal Carbonitride Ti_3CNT_x (MXene). *Science* **2020**, *369* (6502), 446−450.
(36) Park, S. I.; Ahn, J. H.; Feng, X.; Wang, S.; Huang, Y.; Rogers, J. A. Theoretical and Experimental Studies of Bending of Inorganic Electronic Materials on Plastic Substrates. *Adv. Funct. Mater.* **2008**, *18* (18), 2673−2684.
(37) Cao, W. T.; Ma, C.; Mao, D. S.; Zhang, J.; Ma, M. G.; Chen, F. MXene-Reinforced Cellulose Nanofibril Inks for 3D-Printed Smart Fibres and Textiles. *Adv. Funct. Mater.* **2019**, *29* (51), 1905898.
(38) Ma, Z.; Kang, S.; Ma, J.; Shao, L.; Wei, A.; Liang, C.; Gu, J.; Yang, B.; Dong, B.; Wei, L.; Ji, Z. High-Performance and Rapid-Response Electrical Heaters Based on Ultraflexible, Heat-Resistant, and Mechanically Strong Aramid Nanofiber/Ag Nanowire Nanocomposite Papers. *ACS Nano* **2019**, *13* (7), 7578−7590.

https://dx.doi.org/10.1021/acsnano.0c07352
ACS Nano 2021, 15, 829−839